Applied Clay Science 95 (2014) 191–196

Contents lists available at ScienceDirect

Applied Clay Science

journal homepage: www.elsevier.com/locate/clay

Research paper

# Allophane–Pt nanocomposite: Synthesis and MO simulation

Shuichi Arakawa *, Yoko Matsuura, Masami Okamoto *

*Advanced Polymeric Nanostructured Materials Engineering, Graduate School of Engineering, Toyota Technological Institute, 2-12-1 Hisakata, Tempaku, Nagoya 468 8511, Japan*

ARTICLE INFO

*Article history:*
Received 7 February 2014
Received in revised form 5 April 2014
Accepted 9 April 2014
Available online 3 May 2014

*Keywords:*
Synthetic allophane
Pt nanoparticles
Nanocomposite
MO simulation

ABSTRACT

Allophane nanoparticles were synthesized through a hydrothermal treatment of precursor with Si/Al molar ratio of 0.75 at 100 °C for 48 h and characterized by using field emission scanning electron microscopy, pore-size distribution based on the Cranston–Inkley method, $^{29}Si$ and $^{27}Al$ magic angle spinning nuclear magnetic resonance, X-ray diffractometry, and energy dispersive X-ray spectroscopy. It is demonstrated that the synthetic allophane nanoparticle leads to a novel allophane–Pt nanocomposite with the metal particle size of ~2 nm and narrow size distribution. The synthetic allophane particles promote the reduction of $K_2PtCl_4$ to $Pt^0$ and act as a support substratum. The molecular orbital computer simulation was performed to provide insight into the structure and stability of Pt nanoparticles during complexation by the functional $(OH)Al(OH_2)$ groups on the wall perforations of the synthetic allophane.



## 1. Introduction

Novel Pt nanoparticles immobilized on nanoporous materials with high surface area have been extensively investigated during recent decades (Chen and Holt-Hindle, 2010; Su et al., 2010; Sun et al., 2011). Especially, the nanocomposites consisting of Pt nanoparticles and inorganic clay have a great deal of future promise for potential applications as heterogeneous catalysis (Narayanamoorthy et al., 2012; Varade and Hagaguchi, 2013; Zhang et al., 2008). Significant performances have been observed in these catalysts. One promising structure of Pt nanoparticles dispersed on the clay minerals, *e.g.*, montmorillonite and hectorite is a narrow size distribution; $Pt^0$ with the metal particle size of 2–7 nm is believed to be the active site in the Pt-dispersed catalysts. The catalytic efficacy may be gained by tuning specific surface area via consideration of its particle size. Therefore, well-controlled particle sizes and structures of the dispersed Pt nanoparticles must be required.

In the previous example of this issue, Varade and Hagaguchi (2013) examined the synthetic hectorite-mediated synthesis of Pt nanoparticles at room temperature without a strong reducing agent (intricate multistep synthesis). This elegant study demonstrated that difference in nanostructure and composition of clay minerals could influence stability of the Pt nanoparticles (aggregation in solution) and, in turn the metal particle size and size distribution. Because of the high cost of Pt, optimizing both size and shape of the Pt nanoparticles is an issue to be resolved to reduce Pt loading.

In this regard, allophane is the nanoporous material of choice for a functionalized support with high surface area because of its ability in adsorbing cations (*e.g.*, $Cu^{2+}$), anions (*e.g.*, phosphate and arsenate), and organic molecules. Allophane is a short-range-order clay mineral and occurs in some soils derived from volcanic ejecta. The primary particles of the allophane are hollow spherules with an outer diameter of 3.5–5.0 nm and a perforated wall about 0.6–1.0 nm thick (as shown in Fig. 1a) (Brigatti et al., 2006; Matsuura et al., 2013). The specific surface area of allophane single particle is as high as ~900 $m^2/g$, which is often larger than that of activated carbon. Further, the $(OH)Al(OH_2)$ groups exposed on the wall perforations are the source of the pH-dependent charge characteristics of allophane. They become $^{+}(OH_2)Al(OH_2)$ by acquiring protons on the acidic side of the point of zero charge (PZC), and become $(OH)Al(OH)^{-}$ by losing protons on the alkaline side (Kawachi et al., 2013).

In this study, the synthetic allophane nanoparticle is shown to lead to a novel allophane–Pt nanocomposite (APtN) with the metal particle size of ~2 nm and narrow size distribution. In addition, the molecular orbital (MO) computer simulation is performed to provide insight into the structure and stability of the Pt nanoparticle during complexation by the $(OH)Al(OH_2)$ groups.

## 2. Experimental section

### 2.1. Materials and synthetic procedure

#### 2.1.1. Synthesis of allophane

The precursor gel (Si/Al molar ratio = 0.75) for the allophane synthesis was prepared by mixing and stirring (for 1 h) of aqueous solutions (100 mM) of sodium silicate, ortho ($NaSiO_4$, Nacalai-Tesque) and aluminum chloride hexahydrate ($AlCl_3 \cdot 6H_2O$, Sigma-Aldrich). The sodium chloride formed was removed by centrifugation at a speed of 5000 rpm for 5 min. The precursors were then autoclaved at 100 °C

* Corresponding authors. Tel.: +81 528091861; fax: +81 528091864.
*E-mail addresses:* arakawa@toyota-ti.ac.jp (S. Arakawa), okamoto@toyota-ti.ac.jp (M. Okamoto).

http://dx.doi.org/10.1016/j.clay.2014.04.012
0169-1317/

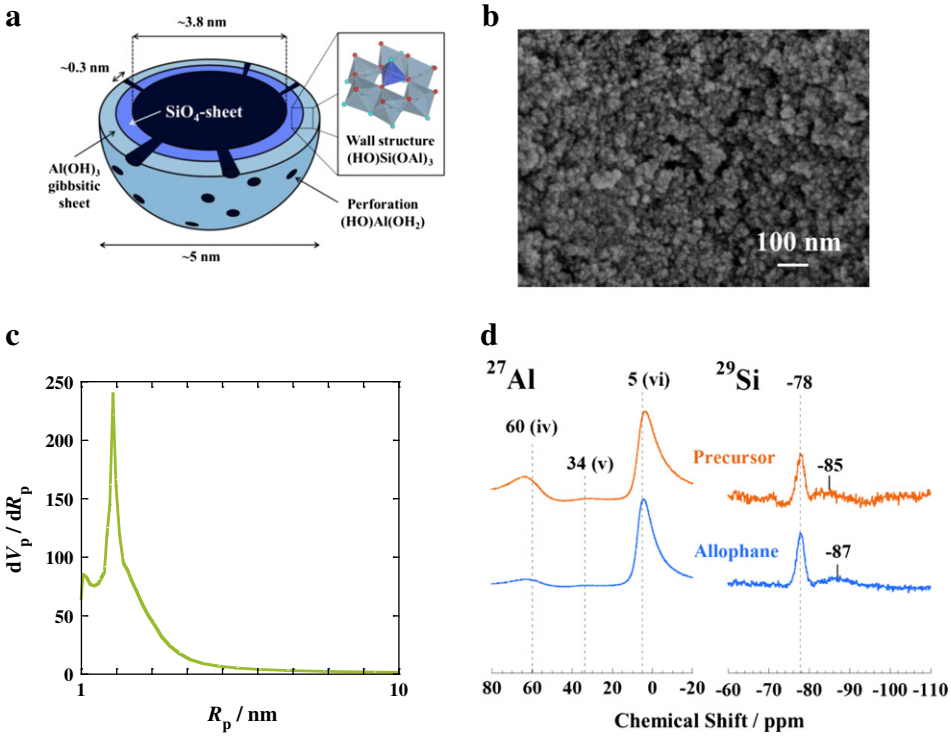


**Fig. 1.** (a) Schematic representation of allophane structure. The overall size of a single allophane particle is ~5 nm. (b) FE-SEM image showing synthetic allophane with Si/Al ratio of 0.82. (c) Pore radius–size distributions of synthetic allophane with Si/Al ratio of 0.82. (d) $^{27}$Al and $^{29}$Si MAS solid-state NMR spectra of precursor gel and synthetic allophane. The data on Y-axis were shifted to avoid overlapping.

for 48 h (Iyoda et al., 2012). Millipore Milli Q ultrapure (18 MΩ cm, total organic carbon (TOC) <20 ppb, Merck Millipore Co. Japan) water through dialysis membrane was used in all experiment.

*2.1.2. Synthesis of allophane–Pt nanocomposite (APtN)*

The synthetic allophane was dispersed in aqueous solution (5.0 mg/mL) using a magnetic stirrer at room temperature for 20 min. In addition 240 μL of aqueous solution of potassium tetrachloroplatinate (II) (5 mass%) ($K_2PtCl_4$, Wako Pure Chemical Industries, Japan) was mixed dropwise (approximately 15 min). The molar ratio of Pt/(Si + Al) in the starting solution was 0.015. The reaction progress was monitored by the color change of the solution from light yellow to black during vigorous 24 h-stirring. After the reaction for 24 h, all the dissolved metal sources were completely deposited. The product was collected by centrifugation at 5000 rpm for 10 min and residual chemical species (such as $Cl^-$) were removed by three consecutive washing/centrifugation cycles with water. The collected product was dried in a vacuum at 45 °C for 48 h. Roughly 0.1 g of product (APtN) was created.

For comparison, the Pt nanoparticles were also tried to prepare without the synthetic allophane by using the same procedure.

*2.2. Characterization*

The morphological features of the synthetic allophane with Si/Al ratio of 0.75 was observed by field emission scanning electron microscopy (FE-SEM) (S-4700, Hitachi Ltd.) equipped with elemental analysis by energy dispersive X-ray spectroscopy (EDX) (EMAX-7000, Horiba Ltd.) after the samples were sputter-coated with platinum under an argon pressure of 10 Pa for 1 min at a current of 10 mA. The average value of the particle size was estimated from the SEM image as described by Sinha et al. (2003).

The pore volume and pore size distribution were measured by the Cranston–Inkley (CI) method (Cranston and Inkley, 1957) using a nitrogen adsorption–desorption approach (BELSORP-mini, Bel Japan, Inc.). The specific surface area was estimated by the *t*-method (Lippens and de Boer, 1965).

The chemical and structural surroundings of both Si and Al ions were measured using $^{27}$Al and $^{29}$Si magic angle spinning (MAS) solid-state nuclear magnetic resonance (NMR). The $^{27}$Al and $^{29}$Si solid-state MAS NMR spectra were collected with a Varian Unity INOVA 400 spectrometer (9.4 T) equipped with 4-mm and 7.5-mm chemagnetics double-resonance MAS probes, respectively. The resonance frequencies at this magnetic field were 104.19 MHz for $^{27}$Al and 79.44 MHz for $^{29}$Si (Iyoda et al., 2012).

The morphology of the product (APtN) was observed through transmission electron microscopy (TEM) (H-9000NAR, Hitachi High-Technologies Co., Japan) operated at an accelerating voltage of 200 kV. The sample (1 mass% in Milli Q ultrapure water) was prepared on copper grids with 300 mesh size, and then water was removed by placing filter paper at the edge of the grids. The particle size was surveyed for more than 150 Pt nanoparticles and analyzed by ImageJ software (U.S. National Institutes of Health).

Wide angle X-ray diffraction (XRD) analysis was performed for the synthetic allophane and APtN, using an X-ray diffractometer (Rigaku Co; 18 kW, graphite monochromator, CuKα radiation (λ = 0.154 nm), operated at 40 kV and 200 mA) at room temperature. Samples were scanned in fixed time mode with counting time of 0.2 s under diffraction angle 2θ in the range of 2–90°.

XPS spectra of APtN were recorded with a Quantera SXM spectrometer (ULVAC-PHI Inc., Japan) using Al Kα radiation (1486.6 eV). Charge neutralization was performed with an electron flood gun and the XPS spectra were calibrated by the Al(2s) peak at 119.6 eV to compensate the charge effect. For the XPS analysis, the experimental data were curve-fitted with Gaussian peaks after subtracting a linear background. The concentration of different states was estimated from the area of the respective Gaussian peaks.

The surface charge characteristics of the synthetic allophane and APtN in water (0.1 mass%) were determined by electrophoresis

(Zetasizer Nano ZS, Malvern Instruments, UK) by the technique of laser Doppler anemometry. The method involved washing allophane several times with water and adjusting the pH of the suspension in the range of 2–11 using dilute $HNO_3$ (Nacalai Tesque Inc.) and NaOH (Nacalai Tesque Inc.).

### 2.3. Model construction

Molecular mechanics force field (MM3) (Scigress, v 2.5.0, Fujitsu Ltd.) has been used for the model construction (Takeshita et al., 2013). In this study, to close up the complexation characteristics, the following solvolysis reactions were used (Ciacchi et al., 2001):

$$PtCl_4^{2-} + H_2O \leftrightarrows PtCl_3(H_2O)^- + Cl^- \quad (1)$$

$$PtCl_3(H_2O)^- + H_2O \rightleftarrows PtCl_2(H_2O)_2 + Cl^-. \quad (2)$$

For this reason, the results obtained from the simulation of the systems were compared between the cases of $PtCl_2(H_2O)_2$ ($Pt^{2+}$) and Pt metal ($Pt^0$) as shown in Fig. 5.

By taking their van der Waals radii into account, the optimization of the molecular structure was based on the minimization of the total energy of the molecular system. The charge densities of each atom were estimated by MO program using a semiempirical parametric method (PM6) (Scigress, v 2.5.0, Fujitsu Ltd.) (Stewart, 2007).

The unit formula of allophane is written as $(OH)_3Al_2O_3Si_{1.2}OH$, which shows Al/Si ratio of 1.72, and indicates the fragments having the imogolite atomic structure over a short range (Parfitt and Henmi, 1980). The fragment links to give a porous and hollow spherule. The ~0.7 nm thick spherule wall is composed of an outer Al octahedral (gibbsitic) sheet and an inner Si sheet, in which the wall structure consists of Si tetrahedral attached to three aluminol groups (Al–OH) of the gibbsite sheet and one silanol group ($HOSi(OAl)_3$).

For this reason, the six constitutive repeating units (CRU) were polymerized to a modeled allophane (m-All) particle having a perforation with six $(OH)Al(OH_2)$ groups, and the overall system was built (inset in Fig. 5a).

The most crucial and important aspect of these calculations is the method selected for sampling the relevant configurational phase space. Accordingly, the conformational search was carried out with MM/MO protocol, in which the relaxed structures were subjected to repeat all the simulations (Mizuno et al., 2013; Takeshita et al., 2013).

## 3. Results and discussion

### 3.1. Synthetic allophane and structural analyses

The FE-SEM image of the synthesized allophane clearly shows the spherical nature of allophane with a mean size of 22.9 ± 4.2 nm (Fig. 1b). The average particle size was much larger than that of the primary particles of allophane because of aggregation caused by the low zeta potential value in the pH 6.5 (Fig. S2) (Iyoda et al., 2012). The EDX spectrum of the allophane sample confirmed the Si/Al molar ratio of 0.82 (image not shown).

The nitrogen adsorption–desorption isotherms of the synthetic allophane (Fig. S1) was type IV isotherms with some hysteresis loop indicating mesopores (Mohanan et al., 2005). The pore radius–size distribution of the synthetic allophane showed a peak at ~1.9 nm (Fig. 1c).

For $^{27}Al$ and $^{29}Si$ MAS NMR measurement (Fig. 1d), the peak at −78 ppm of the $^{29}Si$ spectrum corresponds to the wall structure ($(HO)Si(OAl)_3$) consisting of Si tetrahedra attached to three aluminol groups (Al–OH) of the gibbsite sheet and one silanol group ($Q^3 3^{vi}Al$) (Engelhardt, 1996). In the notation $Q^n$, $Q$ is the Si atom bound to four O atoms with a tetrahedral structure and n indicates the connectivity. No significant peak shift at −78 ppm was observed for the precursor and the synthetic allophane. There is a broad resonance between −83 and −89 ppm. These peaks may suggest that the different chemical structure surroundings of the Si atoms shift the resonance to higher or lower values with the number of Al atoms bound to the central Si atom. The major chemical shifts of $Q^3 1^{vi}Al$ (−84 to −91 ppm) and $Q^3 2^{vi}Al$ (−81 to −86 ppm) are due to the formations on the convex surface of the spherule wall of the synthetic allophane with Si/Al ratio of 0.82.

In the $^{27}Al$ NMR spectra, the 5 ppm peak indicates Al atoms with octahedral coordination ($^{vi}Al$) while the peak at 60 ppm corresponds to tetrahedrally coordinated Al atoms ($^{iv}Al$) (Hiradate and Wada, 2005). The $^{iv}Al$ atoms are substituting the Si atoms of the inner-sheet. A weak peak at 34 ppm in the spectra of the precursor indicates fivefold coordinate Al atoms of the disordered structures. Due to the structural transformations of the precursor into the allophane, the ratio of both iv and v Al atoms decreased.

### 3.2. Synthesis of APtN

For the preparation of APtN, Pt/(Si + Al) molar ratio in the starting solution was fixed at 0.015. The reaction progress was monitored by the color change of the solution from light yellow to black during vigorous 24 h-stirring, indicating that the reduction of $Pt^{2+}$ to $Pt^0$ had occurred. The result shown in Fig. 2a suggests that homogeneous

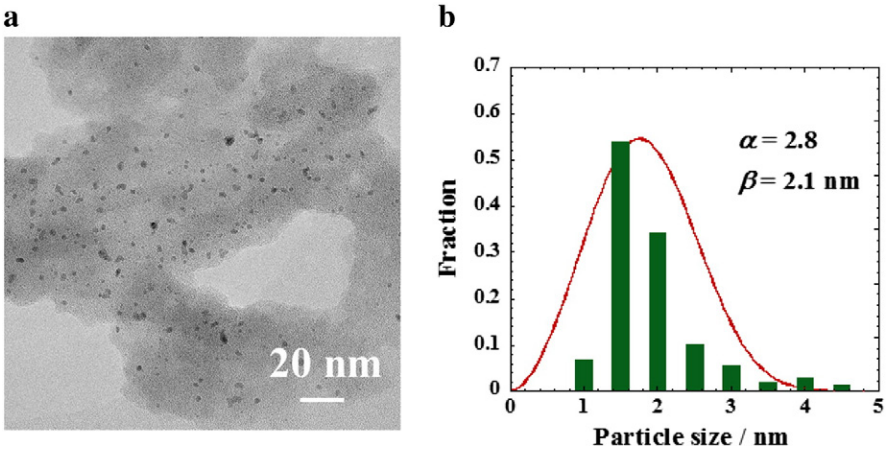


**Fig. 2.** (a) TEM image of APtN with Pt/(Si + Al) molar ratio of 0.018. (b) Particle size distribution. The curve indicates the fitted Weibull function.

dispersion of the Pt particles (dark spherical dots) across the clustered allophane particles (gray area) was achieved. No Pt nanoparticles are observed outside the allophane surface in Fig. 2a.

The distribution function of the form factors was calculated using the Weibull distribution and the results are presented in Fig. 2b. The Weibull function is defined as follows (Eq. (3)):

$$f(x) = \frac{\alpha}{\beta^{\alpha}} x^{\alpha-1} \exp\left[-\left(\frac{x}{\beta}\right)^{\alpha}\right] \quad (3)$$

where $f(x)$ is the fraction, and $\alpha$ and $\beta$ are the variable numbers. The density of the distribution is almost comparative between Gaussian and Weibull fitting curves. The value of $\beta$ corresponds to an average value of the Gaussian distribution (Mizuno et al., 2013). The particle size is distributed in the range 1–4.5 nm, and the average diameter is 2.1 nm by Weibull fitting curve. A more uniform dispersion of Pt nanoparticles seems to be attained as compared to that of $K_2PtCl_4$/synthetic hectorite system (Varade and Hagaguchi, 2013).

The XRD patterns of the synthetic allophane and APtN showed a broad reflection at $2\theta$ ~26° (0.34 nm) and ~40° (0.23 nm), indicating the amorphous nature. Thus, allophane is more appropriately defined as nanosized, short-range ordered aluminosilicate (Fig. 3).

The standard diffraction pattern of Pt metal corresponding to the face centered cubic (fcc) crystals (JCPDS no: 04-0802) is also presented as reference. The (111) reflection at $2\theta = 39.8°$ corresponding to the fcc crystals was not found in XRD profile due to the low loading and the formation of nanoparticles (less than 5 nm-sized Pt nanoparticles) accompanied with reflection broadening (Pina-Zapardiel et al., 2011).

XPS spectra of the Pt($4d_{5/2}$) core level region in APtN are given in Fig. 4a, indicating peaks due to multiple oxidation states. Through the deconvolution into two sets of peaks at 314.9 for Pt metal and 317.7 eV for PtO ($Pt^{2+}$), Pt nanoparticles are found to be dispersed mostly in $Pt^0$ state (67%) and +2 oxidation state (33%) on the clustered allophane particles. In the Pt($4f_{7/2, 5/2}$) peaks (Fig. 4b), the peaks at 72.8, 76.0 and 71.8, 75.1 eV could be assigned to $Pt^{2+}$ and $Pt^0$, respectively. Al(2p) peak at 74.7 eV assigned to the outer gibbsitic sheet of $Al(OH)_3$ well overlaps with three sets of spin-orbit doublet (Shyu and Otto, 1989). Therefore, a peak of Al(2s) at 119.6 eV was taken into account in XPS analysis (Fig. 4c). The estimated Pt/(Si + Al) molar ratio in APtN is 0.018.

In this study, Pt species are not completely reduced to Pt metal ($Pt^0$). In this regard, it is suspected that $K_2PtCl_4$/synthetic hectorite system also includes some fractions of Pt oxidation states (Varade and Hagaguchi, 2013).

No Pt nanoparticle has formed without allophane support (data not shown). In this study, Pt nanoparticles with particle diameter of ~2 nm and narrow size distribution were successfully prepared through in situ reduction of Pt species assisted by the synthetic allophane particles.

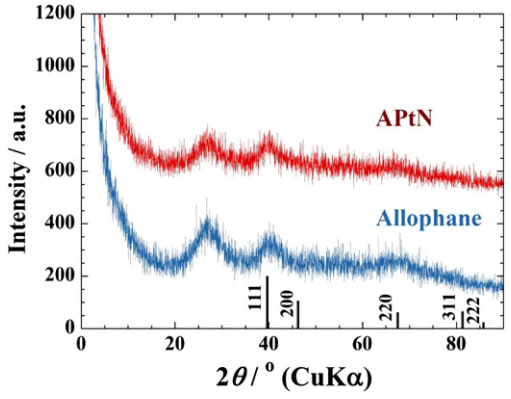


**Fig. 3.** XRD patterns of synthetic allophane with Si/Al ratio of 0.82 and APtN with Pt/(Si + Al) molar ratio of 0.018. Standard diffraction pattern of Pt metal corresponding to the fcc crystals (JCPDS no: 04-0802). The data on Y-axis were shifted to avoid overlapping.

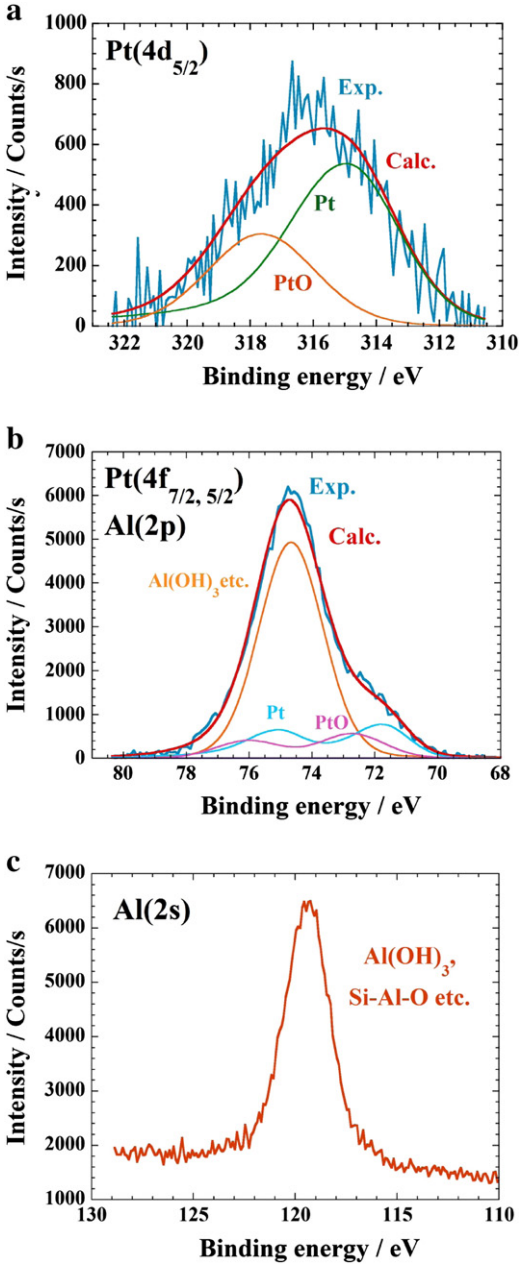


**Fig. 4.** XPS spectra of (a) Pt($4d_{5/2}$), (b) Pt($4f_{7/2, 5/2}$) core level region and Al(2p) peak, and (c) Al(2s) region in APtN.

### 3.3. MO simulation

To further understand the adsorption and reduction processes in the synthesis of APtN, the molecular orbital (MO) computer simulation has been used to probe the structure and stability of Pt nanoparticle during complexation by the functional (OH)Al($OH_2$) groups as neutral site on the PZC. The PZCs of both the synthetic allophane and APtN were (pH) ~7.5, where the (OH)Al($OH_2$) groups act as neutral sites (Fig. S2).

In generating the accurate model of amorphous structure of allophane single particle (m-All) (Fig. 5a and inset), the six CRU, $6((OH)_3Al_2O_3SiOH)$ was built and its geometry optimized by energy minimization. Here the results obtained from the simulation of the systems were compared between the cases of $PtCl_2(H_2O)_2$ ($Pt^{2+}$) (Fig. 5b)

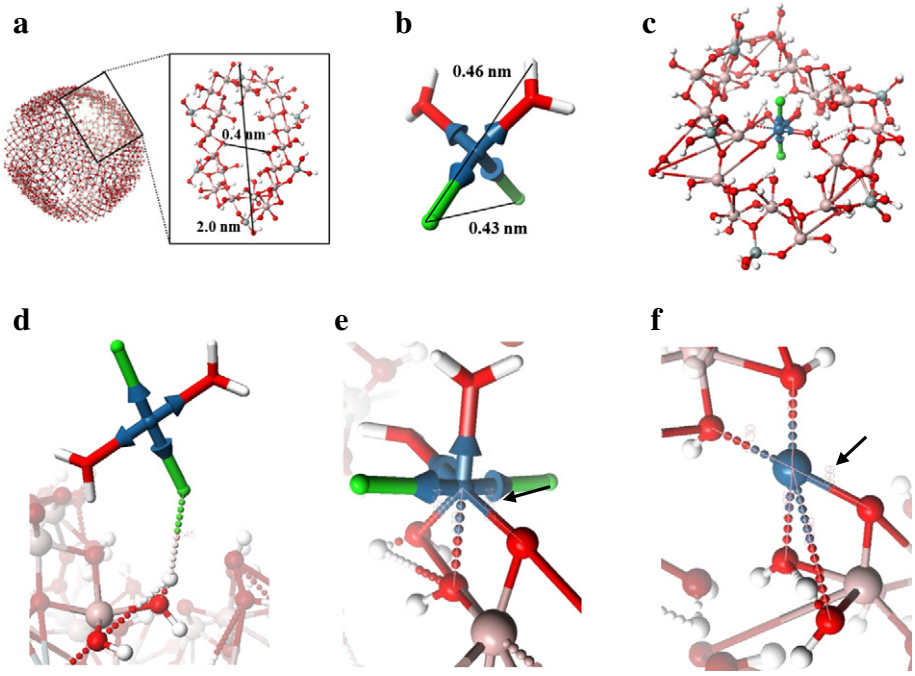


**Fig. 5.** (a) Allophane single particle with amorphous structure and modeled allophane (m-All) fragment having a perforation with six (OH)Al($OH_2$) groups. The dimensions of the wall perforation (length of 20.07 and width of 4.18 Å) of m-All are constructed. (b) Configuration of $PtCl_2(H_2O)_2$ (see model construction). (c) Extracted configuration from the final simulation snapshot of complexation of $PtCl_2(H_2O)_2$ (cylinder model) by m-All (stick and ball model) through Pt···O interaction. Close up of the configuration through Pt–Cl···H–O interaction (d), through Pt···O interaction (e), and complexation of Pt metal by m-All (f). The arrows indicate the formation of new covalent bond of Pt – O. Atom colors: O (red), H (white), Si (light gray), Al (light pink), Cl (green) and Pt (blue).

and Pt metal ($Pt^0$). The mechanism for the reduction may involve the solvolysis reactions of $K_2PtCl_4$. Taking the corresponding configuration between $Pt^{2+}$ and/or $Pt^0$, and the functional (OH)Al($OH_2$) groups of m-All the stable configuration based on the minimization of the total energy was extracted from the final simulation snapshot (Fig. 5c). The conformation is conserved over the duration of MO simulation, indicating that the minimization of the total energy regarding heat of formation is arisen from adopting this new configuration.

### 3.4. Adsorption enthalpy

The heat of formation calculated by using PM6, in which the dominant interactions are electrostatic, as is the case here, was used for estimating the adsorption enthalpy. Taking the adsorption enthalpy ($\Delta H_{ads}$) between Pt species and m-All the stable configuration based on the minimization of the total energy was extracted from the final simulation snapshot. The $\Delta H_{ads}$ values are calculated by using the following equation:

$$\Delta H_{ads} = \Delta H_{complex} - \left(\Delta H_{Pt\ species} + \Delta H_{m\text{-}All}\right) \quad (4)$$

where the $\Delta H_{complex}$ value is the heat of formation (in kcal $mol^{-1}$) of the complexes (such as $PtCl_2(H_2O)_2$–m-All or $Pt^0$–m-All) after adsorption, and $\Delta H_{Pt\ species}$ and $\Delta H_{m\text{-}All}$ are those of the isolated components of Pt species and allophane, respectively.

The calculated results show that the adsorption enthalpy ($\Delta H_{ads}$) (Table 1) value of the complexation through Pt···O interaction (Fig. 5e) is more attractive as compared with that through Pt–Cl···H–O interaction (Fig. 5d). This involves the formation on new covalent bond of Pt – O (marked with the arrow in Fig. 5e). On the other hand, the $\Delta H_{ads}$ value of the complexation with $Pt^0$ shows the largest value (−153.1 kcal/mol) (Table 1), indicating that the strong attractive force is generated between the Pt metal and functional (OH)Al($OH_2$) group, accompanied with Pt – O (covalent) bonding (Fig. 5f). These values display the extent of the differences caused by the stabilized structure after complexation on m-All. Our simulation (PM6) also predicts the average bond distances of Pt···O to be 2.24 for $PtCl_2(H_2O)_2$–m-All (Fig. 5e) and 2.06 Å for $Pt^0$–m-All (Fig. 5f), respectively. The latter exhibits a much shorter distance than that of $PtCl_2(H_2O)_2$ complexes; therefore, the Pt particle effectively pinned to the site by the four Pt···O interaction and $Pt^0$–m-All (Fig. 5f) seems to be stabilized. The reduction of Pt may proceed via complexation as shown in Fig. 5e. The resulting APtN involving the $Pt^0$ state and Pt–O ($Pt^{2+}$) (Fig. 4a) and the obtained particle diameter (~2.1 nm) (Fig. 2b) is the direct evidence of the aggregates of $Pt^0$ atom (diameter of 0.35 nm), which is synthesized on the wall perforations.

## 4. Conclusions

The allophane with Si/Al molar ratio of 0.82 was synthesized by a hydrothermal reaction. The synthetic allophane was poorly crystalline and consisted of hollow spherules with the internal diameter of ~3.8 nm and the characteristic wall structure composed of (HO)Si(OAl)$_3$ groups. The synthetic allophane particles promote the reduction of $K_2PtCl_4$ to $Pt^0$ and act as a support substratum during mechanical agitation of the dispersion. A novel allophane–Pt nanocomposite with the metal particle size of ~2 nm and narrow size distribution was created. These reported

**Table 1**
Heat of formation, adsorption enthalpy of complexes, and bond distances.

| Complexes in Fig. 5 | Heat of formation/kcal/mol | | | $-\Delta H_{ads}$ | Bond distances[a] |
|---|---|---|---|---|---|
| | Allophane | $PtCl_2(H_2O)_2$ or Pt | Complexes | kcal/mol | Å |
| d | | −130.1 | −5354.7 | 17.0 | 3.05 |
| e | −5207.6 | −130.1 | −5403.2 | 65.5 | 2.24 |
| f | | 147.1 | −5213.6 | 153.1 | 2.06 |

[a] The average values of the bond distances are shown.

results demonstrate the first success in preparing APtN with deep insights into molecular level information as revealed by MO simulation.

## Author contributions

S. A. planned the study. Y. M and S. A. performed adsorption and characterization experiments. Y.M. carried out the computer simulation and analyzed the data with the help of S. A. and M. O. The manuscript was written through contributions of all authors. All authors have given approval to the final version of the manuscript.

## Notes

The authors declare no competing financial interest.

## Acknowledgments

This work was supported by the Grant in TTI as a Special Research Project (2012–13) and the Strategic Research Infrastructure Project of the Ministry of Education, Sports, Science and Technology, Japan (2010–14).

## Appendix A. Supplementary data

Nitrogen adsorption–desorption isotherms of synthetic allophane and surface charge characteristics of synthetic allophane and APtN in water. This material is available free of charge via the Internet at http://dx.doi.org/10.1016/j.clay.2014.04.012.

## References

Brigatti, M.F., Galan, E., Theng, B.K.G., 2006. Structure and mineralogy of clay minerals. In: Bergaya, F., Theng, B.K.G., Lagaly, G. (Eds.), Handbook of Clay Science. Elsevier, Amsterdam, pp. 19–86.

Chen, A., Holt-Hindle, P., 2010. Platinum-based nanostructured materials: synthesis, properties, and application. Chem. Rev. 110, 3767–3804.

Ciacchi, L.C., Pompe, W., Vita, A.D., 2001. Initial nucleation of platinum clusters after reduction of $K_2PtCl_4$ in aqueous solution: a first principles study. J. Am. Chem. Soc. 123, 7371–7380.

Cranston, R.W., Inkley, F.A., 1957. The determination of pore structures from nitrogen adsorption isotherms. Adv. Catal. 9, 143–154.

Engelhardt, G., 1996. Silicon-29 NMR of solid silicates. In: Grant, D.M., Harris, R.K. (Eds.), Encyclopedia of Nuclear Magnetic Resonance, 7. John Wiley & Sons, Chichester, pp. 4398–4407.

Hiradate, S., Wada, S.I., 2005. Weathering process of volcanic glass to allophane determined by $^{27}Al$ and $^{29}Si$ solid-state. Clays Clay Miner. 53, 401–408.

ImageJ was written by Wayne Rasband at the U.S. National Institutes of Health. and is available via internet at http://rsb.info.nih.gov/ij (ImageJ is in the public domain).

Iyoda, F., Hayashi, S., Arakawa, S., Okamoto, M., 2012. Synthesis and adsorption characteristics of hollow spherical allophane nano-particles. Appl. Clay Sci. 56, 77–83.

Kawachi, T., Matsuura, Y., Iyoda, F., Arakawa, S., Okamoto, M., 2013. Preparation and characterization of DNA/allophane composite hydrogels. Colloids Surf. B 112, 429–434.

Lippens, B.C., de Boer, J.H., 1965. Studies on pore systems in catalysts: V. The t method. J. Catal. 4, 319–323.

Matsuura, Y., Iyoda, F., Arakawa, S., Okamoto, M., 2013. DNA adsorption characteristics of hollow spherule allophane nano-particles. Mater. Sci. Eng. C 33, 5079–5083.

Mizuno, C., John, B., Okamoto, M., 2013. Percolated network structure formation and rheological properties in nylon 6/clay nanocomposites. Macromol. Mater. Eng. 298, 400–411.

Mohanan, J.L., Arachchige, I.U., Brock, S.L., 2005. Porous semiconductor chalcogenide aerogels. Science 307, 397–400.

Narayanamoorthy, B., Datta, K.K.R., Eswaramoorthy, M., Balaji, S., 2012. Improved oxygen reduction reaction catalyzed by Pt/clay/Nafion nanocomposite for PEM fuel cells. ACS Appl. Mater. Interfaces 4, 3620–3626.

Parfitt, R.L., Henmi, T., 1980. Structure of some allophanes from New Zealand. Clays Clay Miner. 28, 285–294.

Pina-Zapardiel, R., Montero, L., Esteban-Cubillo, A., Moya, J.S., Kaplan, W.D., Paramasivam, T., Pecharromanm, C., 2011. Palladium nanoparticles on silica-rich substrates by spontaneous reduction at room temperature. J. Nanopart. Res. 13, 5239–5249.

Shyu, J.Z., Otto, K., 1989. Characterization of Pt/γ-alumina catalysts containing ceria. J. Catal. 115, 16–23.

Sinha, R.S., Yamada, K., Okamoto, M., Ogami, A., Ueda, K., 2003. New polylactide/layered silicate nanocomposites.3. High-performance biodegradable materials. Chem. Mater. 15, 1456–1465.

Stewart, J.J.P., 2007. Optimization of parameters for semiempirical methods V: modification of NDDO approximations and application to 70 elements. J. Mol. Model. 13, 1173–1213.

Su, F., Poh, C.K., Tian, Z., Xu, G., Koh, G., Wang, Z., Liu, Z., Lin, J., 2010. Electrochemical behavior of Pt nanoparticles supported on meso- and microporous carbons for fuel cells. Energy Fuels 24, 3727–3732.

Sun, S., Zhang, G., Geng, D., Chen, Y., Li, R., Cai, M., Sun, X., 2011. A highly durable platinum nanocatalyst for proton exchange membrane fuel cells: multiarmed starlike nanowire single crystal. Angew. Chem. Int. Ed. 50, 422–426.

Takeshita, T., Matsuura, Y., Arakawa, S., Okamoto, M., 2013. Biomineralization of hydroxyapatite on DNA molecules in SBF: morphological features and computer simulation. Langmuir 29, 11975–11981.

Varade, D., Hagaguchi, K., 2013. Synthesis of highly active and thermally stable nanostructured Pt/clay materials by clay-mediated in situ reduction. Langmuir 29, 1977–1984.

Zhang, W., Li, M.K.S., Yue, P.L., Gao, P., 2008. Exfoliated Pt–Clay/Nafion nanocomposite membrane for self-humidifying polymer electrolyte fuel cells. Langmuir 24, 2663–2670.